# Supplementary Information for "Flow transitions and length scales of a channel confined active nematic"

Abhik Samui [a], Julia M. Yeomans [b], Sumesh P. Thampi [c]

[a] *Department of Physics, Indian Institute of Technology Madras, Chennai 600036, India. E-mail: abhiks@physics.iitm.ac.in*

[b] *The Rudolf Peierls Centre for Theoretical Physics, Clarendon Laboratory, Parks Road, Oxford, OX1 3PU, UK. E-mail: julia.yeomans@physics.ox.ac.uk*

[c] *Department of Chemical Engineering, Indian Institute of Technology Madras, Chennai 600036, India. E-mail: sumesh@iitm.ac.in*

October 6, 2021

## S1 Continuum model for active nematohydrodynamics

In the continuum description of active nematics, the total stress comes from three contributions, namely viscous, elastic and active. The contribution that comes from the Newtonian behaviour of the active fluid gives the viscous stress[1],

$$\boldsymbol{\pi}^{viscous} = 2\eta\mathbf{E} \tag{1}$$

where $\eta$ is shear viscosity and $\mathbf{E} = (\boldsymbol{\nabla}\mathbf{u} + \boldsymbol{\nabla}\mathbf{u}^{\top})/2$ is the strain rate tensor, the symmetric part of the velocity gradient tensor.

The second contribution to the total stress comes from the orientational elasticity of the system since the active entities are generally anisotropic in shape (rod-like or disk-like) and they develop an orientational order due to activity[2,3]. Thus, it is necessary to quantify the order in the system, and the role of free energy associated with this ordering. Restricting to nematic order we use a tensor order parameter,

$$\mathbf{Q} = \frac{q}{2}(3\mathbf{nn} - \mathbf{I}), \tag{2}$$

where $q$ is the strength of ordering for a uniaxial nematic at a point (in the continuum approximation), also known as the uniaxial scalar order parameter[4], $\mathbf{n}$, the director field, is a unit vector that represents the average orientational order of the active entities and $\mathbf{I}$ is the identity tensor.

A thermodynamic contribution to the free energy of the system arises from the gradients in the order parameter field, often classified as bend, splay and twist deformations of the director field. Using a single elastic constant approximation which assigns the same strength to different types of deformations in the order parameter field[5,6], the Frank-Oseen free energy density[6,7] can be defined as

$$F = \frac{K}{2}(\boldsymbol{\nabla}\cdot\mathbf{Q})^2. \tag{3}$$

where $K$ is the elastic constant.

Then the total elastic stress arising from the orientational elasticity has the form

$$\begin{aligned}\boldsymbol{\pi}^{elastic} = & -\boldsymbol{\nabla} P + 2\lambda \left(\mathbf{Q}+\frac{\mathbf{I}}{3}\right)(\mathbf{Q}\colon \mathbf{H}) \\ & -\lambda \mathbf{H}\cdot\left(\mathbf{Q}+\frac{\mathbf{I}}{3}\right) - \lambda\left(\mathbf{Q}+\frac{\mathbf{I}}{3}\right)\cdot\mathbf{H} \\ & -\boldsymbol{\nabla}\mathbf{Q}:\left(\frac{\delta \mathscr{F}}{\delta \boldsymbol{\nabla}\mathbf{Q}}\right) + \mathbf{Q}\cdot\mathbf{H} - \mathbf{H}\cdot\mathbf{Q}.\end{aligned} \tag{4}$$

where $\mathscr{F} = \int F\, d^3r$ is the total free energy of the system. In eqn. (4), the term $P$ refers to the isotropic pressure that includes the contribution from the thermodynamic potential $F$, and $\lambda$ is the flow aligning parameter. The parameter $\lambda$ is related to the shape of the active entities and indicates the tumbling or aligning nature of these entities in a background shear flow. $\lambda > 0$ represents elongated or rod-like particles, $\lambda = 0$ is for spherical particles and $\lambda < 0$ represents disk-like particles[8]. $\mathbf{H}$ given in eqn. 4 is the molecular potential field and can be written as variational derivative of the total free energy $\mathscr{F}$,

$$\mathbf{H} = -\frac{\delta \mathscr{F}}{\delta \mathbf{Q}} + \frac{\mathbf{I}}{3}\,\mathrm{Tr}\left(\frac{\delta \mathscr{F}}{\delta \mathbf{Q}}\right). \tag{5}$$

The last contribution, which arises from the force fields generated by the active entities and which distinguishes active liquid crystals from their passive counterparts is the active stress[9]:

$$\boldsymbol{\pi}^{active} = -\zeta \mathbf{Q} \tag{6}$$

where $\zeta$ is the activity coefficient, and $\zeta < 0$ for contractile systems and $\zeta > 0$ for extensile systems. A mixture of actin filaments and myosin motors can behave as contractile active gel[10]. An example of an extensile system is a suspensions of microtubule bundles powered by kinesin motor proteins[11]. In the literature dealing with collective motion of microswimmers, the contractile and extensile systems are known as puller and pusher type swimmers respectively. As an example, the alga *Chlamydomonas* is a contractile (or a puller) and the bacterium *Escherichia coli* is an extensile (or a pusher) swimmer.

Whereas eqns $1,2$ (in the main article) together represent the hydrodynamics of the flow, the order parameter dynamics can be expressed as[6,12]

$$(\partial_t + \mathbf{u}\cdot\boldsymbol{\nabla})\,\mathbf{Q} - \mathbf{S} = \Gamma \mathbf{H} \tag{7}$$

where $\Gamma$ is orientational diffusivity and $\mathbf{S}$ is the generalised advection term

$$\begin{aligned}\mathbf{S} = & (\lambda \mathbf{E} + \boldsymbol{\Omega})\cdot\left(\mathbf{Q}+\frac{\mathbf{I}}{3}\right) + \left(\mathbf{Q}+\frac{\mathbf{I}}{3}\right)\cdot(\lambda\mathbf{E}-\boldsymbol{\Omega}) \\ & -2\lambda\left(\mathbf{Q}+\frac{\mathbf{I}}{3}\right)(\mathbf{Q}:\boldsymbol{\nabla}\mathbf{u}).\end{aligned} \tag{8}$$

In the above equation, $\boldsymbol{\Omega} = \frac{1}{2}(\boldsymbol{\nabla}\mathbf{u}^{\top} - \boldsymbol{\nabla}\mathbf{u})$ is the vorticity tensor, the antisymmetric part of the velocity gradient tensor. This generalised advection term $\mathbf{S}$ represents how the orientational order parameter field is deformed and rotated with the strain rate and vorticity arising from the flow field. We note that eqn. 3 from the main article is repeated as eqn. 7 in the SI.

To summarise, eqn. 1,2 and 3 (in the main article) govern active nematohydrodynamics: the flow field influences the dynamics of the $\mathbf{Q}$ tensor while the passive and active stresses arising from the orientational order affect the fluid flow thus establishing a two way coupling between the flow and the microstructure fields of the active nematic fluid.

# S2 Methods

## S2.1 Simulation domain

The simulation domain is depicted in Fig. S1. The two dimensional system represents the active nematic confined in a channel in the $x-y$ plane. Channel walls are parallel to $x$ axis. The simulation box is discretised into square elements of size ($\Delta x \times \Delta y$). The small black circles represent the grid points ($x_n$,$y_n$).

## S2.2 Discrete Fourier transform

To capture the essential features of the complex flow fields generated by an active nematic fluid in a channel we analyze the velocity field in Fourier space. The channel used in the simulations is periodic only in the $x$-direction (Fig. S1), and therefore, the Fourier transform is applied only in the $x$-direction, on the instantaneous flow fields. However, as described below, we perform this 1-D analysis at all transverse locations, $y$, and at different times, $t$, to calculate an average value, thus obtaining a mean representation of both spatially and temporally varying features of the flow field.

Since the numerical solution is discrete, we employ discrete Fourier transforms (DFT). Consider the velocity field $\mathbf{u}$ as a function of the coordinate $x$, for a given transverse location $y$ in the channel and a fixed time $t$. By Fourier transforming, we can write each component of the velocity field as a superposition of sinusoidal waves. Thus, the $x$ and $y$ components of velocity field $u_x$ and $u_y$ can be written as,

$$\begin{aligned} u_x(x)|_{y,t} &= a_0 + \sum_{k\neq 0} a_k \sin(kx + \psi_{u_x}(k)) \\ u_y(x)|_{y,t} &= b_0 + \sum_{k\neq 0} b_k \sin(kx + \psi_{u_y}(k)) \end{aligned} \tag{9}$$

where $a_0$ and $b_0$ are the amplitudes corresponding to $k = 0$ mode, $a_k$ and $b_k$ are the amplitudes corresponding to the $k^{\text{th}}$ wave number and $\psi_{u_x}(k)$ and $\psi_{u_y}(k)$ are the arbitrary phase factors. The notation $|_{y,t}$ indicates that $u_x$ and $u_y$ are calculated when $y$ and $t$ are fixed. It may be noted that the amplitudes $a_0$ and $b_0$ give the non-oscillatory parts (the constant contributions) of $u_x$ and $u_y$ respectively.

Flow circulations and vortices are characteristic aspects of complex flow states generated by an active nematic fluid. Therefore analyzing the field variable vorticity, defined as the curl of velocity field $\boldsymbol{\omega} = \nabla \times \mathbf{u}$, which quantifies the local rotationality of the fluid elements, is also helpful. In two dimensions, the only non-zero component of vorticity is $\omega_z$, oriented normal to the plane under consideration. This vorticity field can also be Fourier transformed to obtain

$$\omega_z(x)|_{y,t} = c_0 + \sum_{k\neq 0} c_k \sin(kx + \psi_\omega(k)) \tag{10}$$

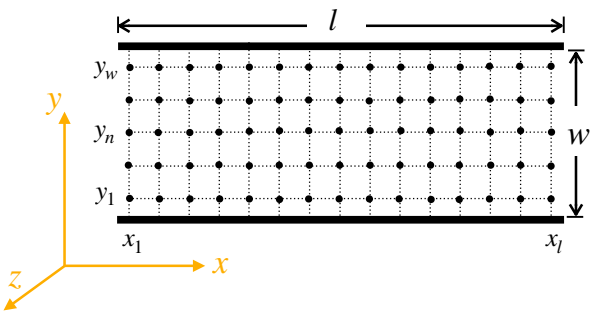


**Figure S1** Schematic of the domain used in the simulations. The domain is periodic along the $x$ direction and confined by parallel plates at the top and bottom, thus representing a two-dimensional channel.

where $c_0$ and $c_k$ are the amplitudes corresponding to $0^{\text{th}}$ and $k^{\text{th}}$ modes respectively and $\psi_\omega(k)$ is the associated arbitrary phase.

Further, it is useful to define two quantities $\phi_0$ and $\phi_k^{max}$ from the Fourier amplitudes of the $x$-component of the velocity field ($u_x$),

$$\phi_0 = [\phi_k]_{k=0} \quad \text{and} \quad \phi_k^{max} = \text{Max}\left[\phi_{k,k\neq 0}\right] \tag{11}$$

where $\phi_k$ is the space-time average of the amplitude $a_k(y_n,t)$ corresponding to $k^{\text{th}}$ mode obtained from the discrete Fourier transform of $u_x(x)$ (defined in eqn (9)). $\phi_k$ is calculated as

$$\phi_k = \frac{1}{m}\sum_{t=t_1}^{t_m}\left(\frac{1}{w}\sum_{n=1}^{w} a_k(y_n,t)\right). \tag{12}$$

In other words, the spatial average of $a_k(y_n,t)$ is taken over $w$ grid points spanning the channel width (in the $y$ direction) and the time average is performed over $m$ snapshots of the velocity field, indicated by $(t_1,t_2,..,t_m)$. In our calculations, we choose $m = 10$. The quantity $\phi_0$ is the space - time average of the Fourier amplitude of the $k = 0$ mode. Physically it represents the average fluid velocity along the channel length (here along the $x$ axis). $\phi_k^{max}$ is the maximum among the averaged amplitudes for $k \neq 0$ modes. This quantity provides the amplitude of the most dominant wave constituting the flows. In our work, we used the Fast Fourier Transform (FFT) technique to calculate the DFT.

This analysis in Fourier space also allows us to identify the characteristic length scale associated with the complex flow fields exhibited by channel-confined active nematics. This characteristic length, $L_F$, is defined as the wavelength $1/k$ (according to the convention adopted in FFT) corresponding to the maximum Fourier amplitude among the $k \neq 0$ modes. Thus, corresponding to the Fourier transform of $u_x$, $u_y$ and $\omega_z$, the three characteristic lengths that emerge in the analysis are

$$L_F^{u_x} = \frac{1}{k_{u_x}^{max}}, \qquad L_F^{u_y} = \frac{1}{k_{u_y}^{max}}, \quad \text{and} \quad L_F^{\omega_z} = \frac{1}{k_{\omega_z}^{max}} \tag{13}$$

where $k_{u_x}^{max}$, $k_{u_y}^{max}$ and $k_{\omega_z}^{max}$ are the wavenumbers corresponding to the maximum in Fourier amplitude. The maxima are identified by analysing the space-time average values of Fourier amplitudes, for example $k_{u_x}^{max}$ is obtained from $\phi_k$ calculated according to eqn 12. A similar procedure is followed to calculate $k_{u_y}^{max}$ and $k_{\omega_z}^{max}$.

## S2.3 Correlation functions

To understand the spatial correlation of the flow fields the following quantities are calculated. Due to the confinement, only the correlation along the channel length ($x$ - direction) is considered. Thus, for two points separated by a distance $r$ along the channel length, the one-dimensional correlation for the longitudinal component of velocity $C_{u_xu_x}(r,t)$, the transverse component of velocity $C_{u_yu_y}(r,t)$, and the vorticity $C_{\omega_z\omega_z}(r,t)$ are defined, respectively, as

$$\begin{aligned}
C_{u_xu_x}(r,t) &= \frac{\langle u_x(x_n,y_n,t)u_x(x_n+r,y_n,t)\rangle}{\langle u_x^2(x_n,y_n,t)\rangle} \\
C_{u_yu_y}(r,t) &= \frac{\langle u_y(x_n,y_n,t)u_y(x_n+r,y_n,t)\rangle}{\langle u_y^2(x_n,y_n,t)\rangle} \\
C_{\omega_z\omega_z}(r,t) &= \frac{\langle \omega_z(x_n,y_n,t)\omega_z(x_n+r,y_n,t)\rangle}{\langle \omega_z^2(x_n,y_n,t)\rangle}.
\end{aligned} \tag{14}$$

Here $\langle ...\rangle$ represents averaging over all points along the $x$ axis. The correlations are calculated for a fixed value of $y_n$ and for a time instant $t$ in the steady states.

For comparison, we also calculate correlation functions of the fluid flows observed in unconfined active nematic systems in two dimensions. Again, defining for the velocity and the vorticity field, they are,

$$C^b_{\mathbf{uu}}(r,t) = \frac{\langle \mathbf{u}(x_n,y_n,t)\cdot\mathbf{u}(x_n+r_x,y_n+r_y,t)\rangle}{\langle u^2(x_n,y_n,t)\rangle}$$
$$C^b_{\omega_z\omega_z}(r,t) = \frac{\langle \omega_z(x_n,y_n,t)\omega_z(x_n+r_x,y_n+r_y,t)\rangle}{\langle \omega_z^2(x_n,y_n,t)\rangle} \tag{15}$$

where $r = \sqrt{r_x^2+r_y^2}$ is the distance between two points in the 2d plane and averaging $\langle ...\rangle$ is done for all the points in that plane.

Similarly to the length scales defined in section S2.2, the correlation functions also provide characteristic length scales of the flow fields. We define the characteristic length $L_c$ as time average of twice the distance $r$ at which the correlation function decays to its first minimum i.e. if $r_{min}$ is the distance where correlation function has its first minimum then we can write $L_c$ as $\langle 2r_{min}(t)\rangle$ where $\langle ...\rangle$ indicates time averaging. Therefore, $L_c$ measures the length over which velocity and vorticity patterns repeat in the flow fields for oscillatory and dancing flow states (see Fig. 1 (b,c) in the main article). The two length scales corresponding to the velocity and vorticity field are denoted as $L_c^{\mathbf{u}}$ and $L_c^{\omega_z}$. In a similar fashion, for confined systems, the characteristic lengths $L_c^{u_x}$, $L_c^{u_y}$ and $L_c^{\omega_z}$ are obtained from the velocity-velocity correlation for $x$ and $y$ components of the velocity field, and the vorticity field respectively.

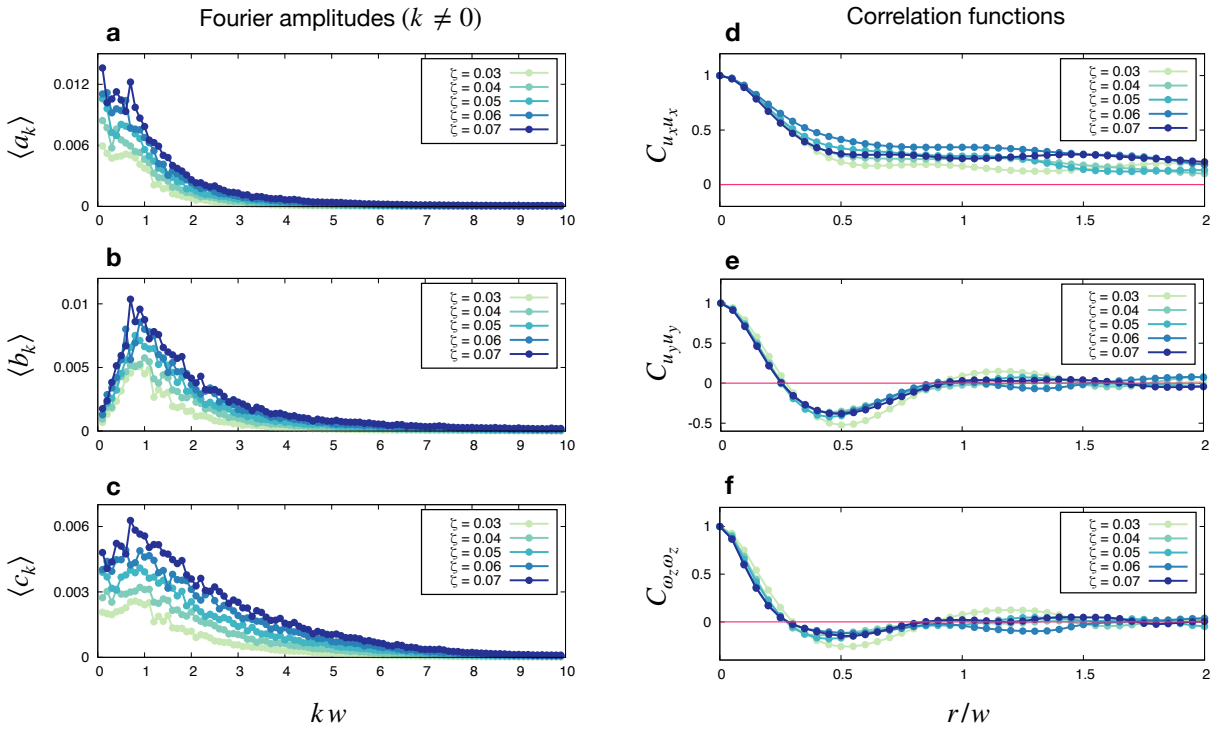


**Figure S2** Fourier amplitudes and correlation functions of the flow field corresponding to localised active turbulence. The left side panels show the space-time average of Fourier amplitudes ($k \neq 0$) (a) $\langle a_k\rangle$, (b) $\langle b_k\rangle$ and (c) $\langle c_k\rangle$ corresponding to $u_x(x)$, $u_y(x)$ and $\omega_z(x)$ respectively, at different activities $\zeta$. Panels on the right hand side shows the corresponding, time-averaged 1D correlation functions. Velocity-velocity correlation functions $C_{u_x u_x}$ and $C_{u_y u_y}$ are shown in (d) and (e) respectively and the vorticity-vorticity correlation $C_{\omega_z\omega_z}$ is shown in (f). Note that the correlation functions are evaluated at a fixed $y$ location, $y_n/w = 0.525$, close to the channel centre line.

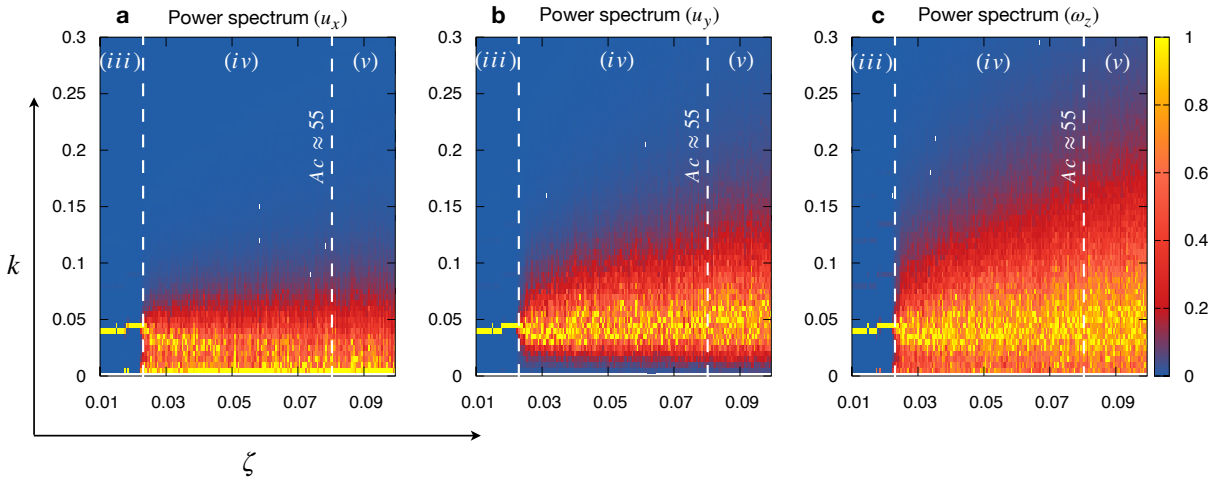


**Figure S3** Normalised power spectra for $u_x$, $u_y$ and $\omega_z$ are shown in the $k-\zeta$ plane in (a), (b) and (c) respectively. In all plots, the base colour blue indicates zero power whereas yellow depicts maximum power. White dashed lines demarcate different flow regions, $(iii)$ dancing flow, $(iv)$ localised active turbulence and $(v)$ fully-developed active turbulence.

## S3 Characteristic lengths of localised active turbulence for varying activity

In Fig. 3, it is shown that both oscillatory and dancing flow states have only one characteristic length scale that can be measured from the Fourier analysis of the flow field, i.e, $L_F^{u_x}$. Similar analysis on $u_y$ and $\omega_z$ show that both $L_F^{u_y}$ and $L_F^{\omega_z}$ are also equal to $L_F^{u_x}$. Moreover, this characteristic length was found to be independent of activity. However such inferences could not be drawn categorically for localised active turbulence as it exhibited a bimodal distribution with only a shallow trough in between the peaks, when $u_x(x)$ was analyzed in Fourier space (Fig. 3 in the main article). Though the overall features of the power spectrum was insensitive to the variation in $\zeta$, it was not possible to identify a characteristic length $L_F^{u_x}$ corresponding to localised active turbulence. The details change as we analyze $u_y(x)$ and $\omega_z(x)$ (see Fig. S3(b,c)) and hence we further analyze the spectrum of velocity field in localised active turbulence in this section. In order to understand the relevance of these length scales and the nature of localised active turbulence in the channel, we also plot the correlation functions of $u_x(x)$, $u_y(x)$ and $\omega_z(x)$.

As shown in Fig. S2(a), the Fourier amplitudes $\langle a_k \rangle$ show a wide span in $k$ space at all activities. The spectra are bimodal as observed earlier in Fig. 3 (in the main article) but the peaks are not very distinct as the Fourier amplitudes are very close to each other. The two peaks in $\langle a_k \rangle$ correspond to two length scales. $(i)$ $kw \approx 0$ represents a length comparable to channel length $(l)$ and $(ii)$ $kw \approx 1.0$ corresponds to a length scale the same as the channel width $w$. An important point to be noted is that, as $\zeta$ increases, $k \approx 0$ becomes the more dominant mode among the two maxima (see Fig. S3(a)). In Fig. S2(b), average Fourier amplitudes $\langle b_k \rangle$ (which correspond to $u_y(x)$) show a different type of spread over $k$ space with a characteristic maximum in the spectrum at all activities. The maxima are located at $kw \approx 1.0$, i.e, at a length scale corresponding to the channel width. Similar to $\langle b_k \rangle$, though less distinct, there exists a peak in $\langle c_k \rangle$ as well, as shown in Fig. S2(c). So to summarise, the analysis of $u_x$ shows that the dominant wavelength corresponds to the channel length or width ($L_F^{u_x} \approx l$ or $w$) whereas analysis of $u_y$ and $\omega_z$ show the dominant lengths as the confinement width ($L_F^{u_y} \approx w$ and $L_F^{\omega_z} \approx w$) for localised active turbulent flows.

In order to gain further physical insights into the range of length scales observed in Fourier space corresponding to localised active turbulence, we now discuss the time averaged 1D correlation

functions, $C_{u_xu_x}$, $C_{u_yu_y}$ and $C_{\omega_z\omega_z}$. All these correlation functions decay with $r$ as shown in Fig. S2(d, e, f). The decay is expected as the velocity and vorticity field associated with localised active turbulent flow are irregular as shown in Fig. 1(d). However there is a distinct difference in the correlation function for $u_x$ compared to that of $u_y$ and $\omega_z$. The correlation functions $C_{u_yu_y}$ and $C_{\omega_z\omega_z}$, shown in Fig. S2(e) and Fig. S2(f) respectively, decay, then cross zero and show a negative correlation before decaying to zero completely. This occurs irrespective of the value of the activity ($\zeta$). In contrast, the correlation functions $C_{u_xu_x}$ shown in Fig. S2(d) reach zero only at much larger distances ($r/w > 2$) for all values of the activity coefficient. In other words, the correlations in $u_x$ can span over long distances, sometimes even comparable to the channel length. The reason for this long ranged correlation in $u_x$ but absent in $u_y$ and $\omega_z$ is likely to be the fluid jets present in the localised active turbulent flow state. It is interesting to note that, for the same reason, the first minima of $C_{u_xu_x}$ are widely scattered between $r/w \approx 0.5$ and $r/w \approx 5.0$. On the other hand, $C_{u_yu_y}$ and $C_{\omega_z\omega_z}$ show well defined first minima at all activities and both correlation functions decay to zero for $r/w > 1$.

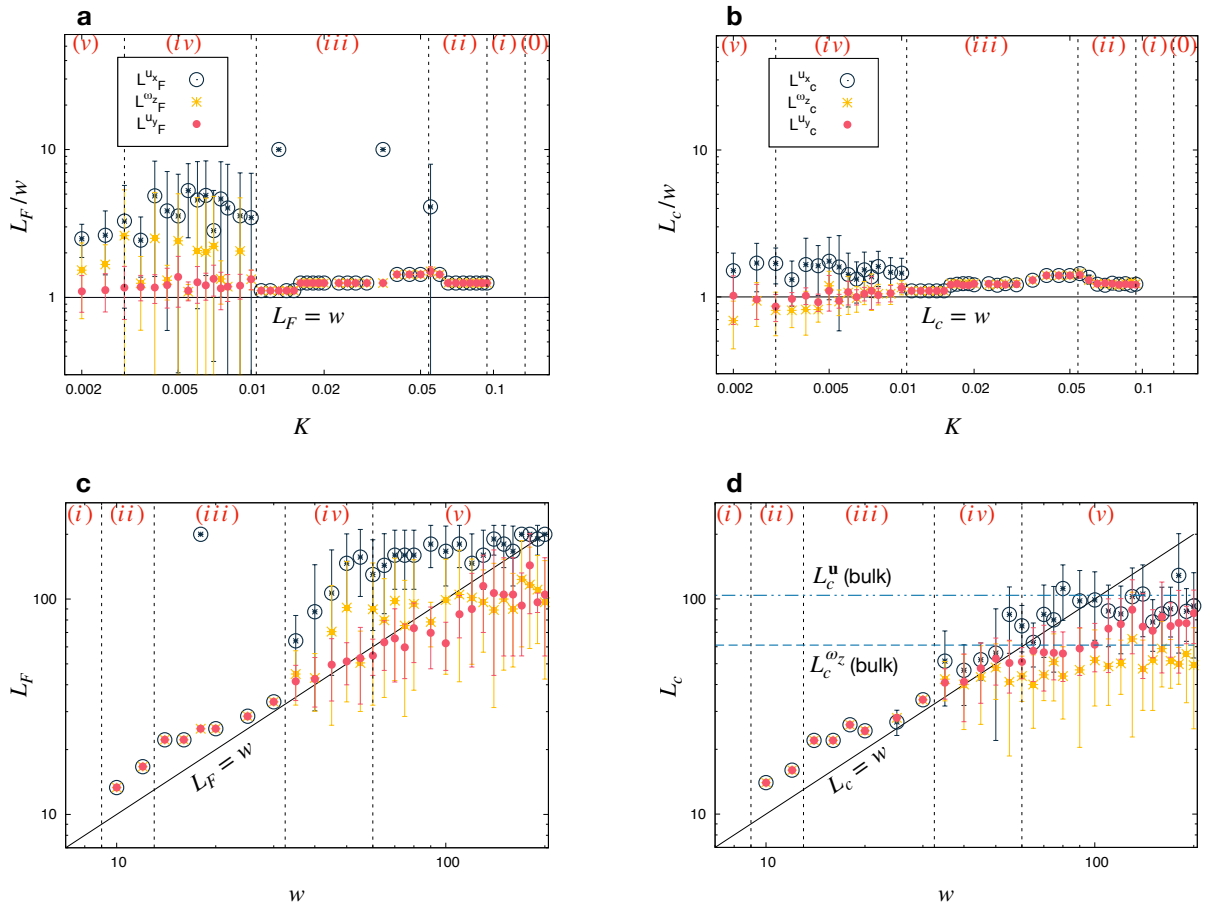


**Figure S4** Characteristic length scales (a) $L_F$ and (b) $L_c$ corresponding to variation in elasticity ($K$) for $\zeta = 0.024$, $l = 200$ and $w = 20$ and length scales (c) $L_F$ and (d) $L_c$ for variation of channel width ($w$) for $\zeta = 0.01$, $K = 0.01$ and $l = 200$. In the left panel $L_F^{u_x}$ (black), $L_F^{u_y}$ (red) and $L_F^{\omega_z}$ (yellow) are extracted from Fourier amplitudes. On the right panel, $L_c^{u_x}$ (black), $L_c^{u_y}$ (red) and $L_c^{\omega_z}$ (yellow) are from correlation functions. $L_F$ and $L_c$ are non-dimensionalised by the channel width $w$ in (a) and (b). The black dashed lines demarcate different flow states, namely (0), ($i$), ($ii$), ($iii$), ($iv$) and ($v$) indicate no flow, unidirectional flow, oscillatory flow, dancing flow, localised active turbulence and fully-developed active turbulent flow respectively.

The characteristic length $L_c^{u_y}$ corresponding to the correlation function $C_{u_yu_y}$ (defined as twice the first minimum) is approximately the same as the channel width, $L_c^{u_y} \approx w$. In other words, the

correlation function for the transverse component of velocity $u_y$ has a characteristic length scale that is comparable to confinement length $w$. A similar behaviour is observed for $L_c^{\omega_z}$, the length scale corresponding to correlation of vorticity. In other words, $L_c^{\omega_z} \approx w$, and the average vortex size (size of a clockwise and an anti-clockwise vortex pair) for localised active turbulent flow in 2D confinement is comparable to the channel width $w$ irrespective of the activity ($\zeta$).

In short, although localised active turbulence is seemingly chaotic, it is still characterised by well-defined length scales under 2D confinement. Analysis in both Fourier space and from correlation functions show that the longitudinal component of velocity $u_x$ exhibits a characteristic length scale ($L_F^{u_x}$ or $L_C^{u_x}$) between the width ($w$) and length ($l$) of the channel while the transverse component $u_y$ and vorticity $\omega_z$ have characteristic dimensions of the width of the channel. Thus, depending upon the analysis, mode of selection and the sample, analysis of $u_x$ gives varying values between $\approx w$ and $\approx l$ while analysis of $u_y$ or $\omega_z$ gives a unique value as the characteristic length scale of the flow.

## S4 Characteristic lengths of flow states when elasticity and channel width are varied

Fig. S4(a, b) illustrate results for the characteristic length scales $L_F$ and $L_c$ when the elasticity $K$ is varied ($\zeta = 0.024$, $l = 200$ and $w = 20$ are kept fixed). For low values of the elastic constant, the active nematic exhibits fully developed turbulent flow (marked as $(v)$). With increase in elasticity, the flow turns to localised active turbulence $(iv)$ and then to dancing $(iii)$, oscillatory $(ii)$, and unidirectional flow $(i)$ followed by a no flow $(0)$ state. Despite these changes in the flow states, it is interesting to note that characteristic lengths of the flow $L_c^{u_x}$, $L_c^{u_y}$ and $L_c^{\omega_z}$ obtained from the correlation functions are again close to the channel width $w$ except in fully developed turbulent flow $(v)$ where the characteristic lengths start decreasing from $w$ as $K$ is decreased. On the other hand, $L_F^{u_x}$, $L_F^{u_y}$ and $L_F^{\omega_z}$ show larger variations from $w$, with values varying between $w$ and $l$.

Fig. S4(c, d) show the variation in $L_F$ and $L_c$ when the width of the channel $w$ is varied but keeping other parameters fixed ($\zeta = 0.01$, $K = 0.01$ and $l = 200$). It may be noted from Fig. S4(d) that the characteristic lengths $L_c$ increase with increasing $w$ up to a certain channel width ($w \approx 60$) beyond which they saturate to a plateau and they do not increase further. The transition from the linear increase with $w$ to the plateau occurs irrespective of whether it is measured from $u_x$, $u_y$ or $\omega_z$. However it is difficult to identify the transition from Fig. S4(c), i.e when length scales are measured from Fourier analysis since $L_F$ is domain size dependent and shows large standard deviations.

Analyzing the transition in Fig. S4(d) more closely, we note that among the all $L_c$, $L_c^{\omega_z}$ is a convenient choice to demarcate the transition to fully developed active turbulence since (i) it starts saturating at the transition point between localised active turbulence and fully developed active turbulence and plateaus at $L_c^{\omega_z}$ (bulk) immediately beyond the transition (ii) the transition occurs when $L_c^{\omega_z} \approx w \approx L_c^{\omega_z}$(bulk). The other two characteristic length scales based on the velocity field $L_c^{u_x}$ and $L_c^{u_y}$ also follow $L_c^{\omega_z}$ but saturate to $L_c^{\mathbf{u}}$ (bulk), the characteristic length scale corresponding the velocity of the bulk fluid.

## S5 Temporal evolution of the characteristic lengths for various flow states

Considering that the flow evolves through different flow states before reaching a final state, and the characteristic length scale does not change for various flow states at steady state, it is natural to ask whether the different unsteady flow states exhibit a single characteristic length scale as well. Therefore we monitor the temporal evolution of the flow before reaching the final steady state of the different flow states. The results are presented in Fig. S5. Here, the characteristic lengths $L_c^{u_x}$, $L_c^{u_y}$ and $L_c^{\omega_z}$, the correlation lengths for $u_x$, $u_y$ and $\omega_z$, are shown as a function of time as the system evolves to a steady state for two different activities (a) $\zeta = 0.005$ and (b) $\zeta = 0.0245$. For $\zeta = 0.005$, the initial no-flow state evolves through a unidirectional and oscillatory flow before

reaching the dancing flow state. Similarly for $\zeta = 0.0245$, the dancing flow prevails for some time before attaining the localised active turbulent state. It is interesting to note that though the active nematic undergoes these flow transition in time, the characteristic length scale corresponding to the different flow states does not change and it remains comparable to the channel width $w$ as shown in Fig. S5. This observation leads us to propose that flow transitions in the channel-confined active nematic are a consequence of instabilities as we discuss in section 3.4.

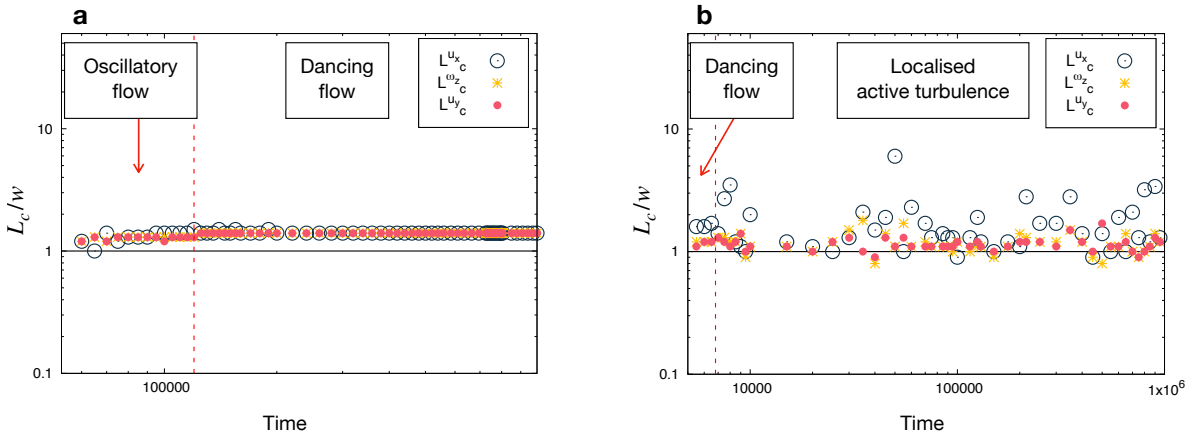


**Figure S5** Characteristic lengths of the flow field generated by a channel-confined active nematic as it evolves from a no flow state to a steady flow state for (a) $\zeta = 0.005$ and (b) $\zeta = 0.0245$. In both panels, the vertical axis represents lengths corresponding to correlation functions and the horizontal axis indicates time. The vertical dashed lines indicates the flow transitions. In (a), the system exhibits an oscillatory state before reaching the dancing state at steady state. In (b) the system exhibits the dancing state before reaching localised active turbulence at steady state.

## Notes and references


[1] G. K. Batchelor, *An introduction to fluid dynamics*, Cambridge Univ. Press, 2000.

[2] S. Santhosh, M. R. Nejad, A. Doostmohammadi, J. M. Yeomans and S. P. Thampi, *J. Stat. Phys.*, 2020, **180**, 699–709.

[3] S. Chandragiri, A. Doostmohammadi, J. M. Yeomans and S. P. Thampi, *Soft Matter*, 2019, **15**, 1597–1604.

[4] T. C. Lubensky, *Phys. Rev. A*, 1970, **2**, 2497–2514.

[5] F. C. Frank, *Discuss. Faraday Soc.*, 1958, **25**, 19–28.

[6] P. D. Olmsted and P. M. Goldbart, *Phys. Rev. A*, 1992, **46**, 4966.

[7] P. G. de Gennes and J. Prost, *The physics of liquid crystals*, Oxford Univ. Press, 1993.

[8] S. A. Edwards and J. M. Yeomans, *Europhys. Lett.*, 2009, **85**, 18008.

[9] R. A. Simha and S. Ramaswamy, *Phys. Rev. Lett.*, 2002, **89**, 058101.

[10] J. Alvarado, M. Sheinman, A. Sharma, F. C. MacKintosh and G. H. Koenderink, *Soft Matter*, 2017, **13**, 5624–5644.

[11] T. Sanchez, D. T. N. Chen, S. J. DeCamp, M. Heymann and Z. Dogic, *Nature*, 2012, **491**, 431–434.

[12] A. N. Beris and B. J. Edwards, *Thermodynamics of flowing systems: with internal microstructure*, Oxford Univ. Press, 1994.